Engineering Analysis with Boundary Elements 33 (2009) 1124–1131

Contents lists available at ScienceDirect

Engineering Analysis with Boundary Elements

journal homepage: www.elsevier.com/locate/enganabound

Computation of singular and hypersingular boundary integrals by Green identity and application to boundary value problems

F. Seydou [a,*], R. Duraiswami [b], T. Seppänen [a], N.A. Gumerov [b]

[a] Department of Electrical and Information Engineering, University of Oulu, P.O. Box 3000, 90401, Finland
[b] Institute for Advanced Computer Studies University of Maryland, College Park, MD, USA

ARTICLE INFO

Article history:
Received 30 October 2007
Accepted 17 February 2009
Available online 6 May 2009

Keywords:
Bounday integral method
Green identity
Singular integrals
Hypersingular integrals
Nyström method

ABSTRACT

The problem of computing singular and hypersingular integrals involved in a large class of boundary value problems is considered. The method is based on Green's theorem for calculating the diagonal elements of the resulting discretized matrix using the Nyström discretization method. The method is successfully applied to classical boundary value problems. Convergence of the method is also discussed.

1. Introduction

The mathematical treatment of the scattering of time-harmonic acoustic or electromagnetic waves by an infinitely long cylindrical obstacle with a simply connected bounded cross-section $\Omega \subset \mathbf{R}^2$, leads to the exterior Helmholtz equation

$$(\Delta + k^2)u = 0 \quad \text{in } \mathbf{R}^2 \backslash \Omega, \tag{1.1}$$

where $k>0$ is the wave number and the field u is decomposed, $u = u^{inc} + u^s$, into the given incident field u^{inc}, which is assumed to satisfy the Helmholtz equation everywhere, except possibly at isolated points in $\mathbf{R}^2$, and the unknown scattered field u^s, which is required to satisfy the Sommerfeld radiation condition

$$\lim_{|\mathbf{x}|\to\infty} |\mathbf{x}|^{1/2}\left(\frac{\partial u^s}{\partial |\mathbf{x}|} - iku^s\right) = 0, \tag{1.2}$$

uniformly in all directions. Depending on the physical nature of the scattering obstacle, the total field u has to satisfy a boundary condition on Γ, the boundary of Ω. Usually the following boundary conditions are considered

1. Dirichlet condition:

$$u = 0; \tag{1.3}$$

2. Neumann condition:

$$\frac{\partial}{\partial v}u = 0, \tag{1.4}$$

where v is the unit outward normal, which is assumed to be directed to the exterior; and

3. Transmission condition:

$$\frac{\partial}{\partial v}u = \rho\frac{\partial}{\partial v}u_i, \tag{1.5}$$

$$u = u_i, \tag{1.6}$$

where ρ is a non-zero complex constant and u_i satisfies the Helmholtz equation in Ω, with k replaced by k_i.

In acoustics the Dirichlet (resp. Neumann) condition corresponds to sound soft (resp. hard), whereas in electromagnetics it models scattering from a perfect conductor with the electromagnetic field H (resp. E)-polarized. The transmission condition corresponds in acoustics (resp. electromagnetics) to the continuity of pressure and normal velocity (resp. scattering from a dielectric).

The problem of determining the unknown function u^s, for the above stated equations, with arbitrary shape of Ω and wave number k, is not an easy task. Usually a tedious and costly numerical calculation is expected.

Many numerical solutions have been considered. The finite element and finite difference methods could be used to compute the unknown field, but they involve a discretization of the two-dimensional (2D) space, which is a heavy numerical task, especially for high wave numbers. Moreover it is impossible to discretize to infinity, and one has either to couple the finite element with boundary element using artificial boundaries or select a cut-off at some arbitrary distance from the obstacle and implement there the Sommerfeld radiation condition (cf. [15] and the references therein).

* Corresponding author.
E-mail address: fadseydou@nepadcouncil.org (F. Seydou).

0955-7997/$ - see front matter © 2009 Elsevier Ltd. All rights reserved.
doi:10.1016/j.enganabound.2009.02.004

One of the most popular strategies in recent years is the plane-wave decomposition method (PWDM) [12,26]. The method is based on the assumption that each (discretized) solution can be approximated by an ansatz of the superposition of plane waves, at a given wave number. The ansatz solves the Helmholtz equation in the discretized system and the boundary condition determines the unknown functions. This method, thus, reduces the calculations to a one-dimensional (1D) boundary grid instead of the 2D space. The problem of creating discretizations ("meshing") is well known to be a difficult task—almost an art, and the simplicity achieved by a reduction in dimensionality must not be underestimated. The PWDM is found to be extremely efficient in practice. However, solutions of non-convex boundaries, in general, cannot be approximated by any solution of the Helmholtz equation regular everywhere (in particular, by linear combinations of a finite number of plane waves having the same energy) [11]. From this we see that PWDM cannot be applied efficiently to important types of shapes.

The main useful numerical strategies that have been suggested in the literature, for arbitrary shapes, are based on boundary integral approach and often referred to as boundary integral method (BIM). This strategy, which requires 1D grid calculations, is very similar to the PWDM. It is also based on the observation that the solutions are completely determined by their behavior at the boundary, and use basis functions that satisfy the Helmholtz equation in the system at fixed wave number. A linear combination of the basis functions is then selected such that the boundary conditions are satisfied. The method is derived from exact integral equation using Green's theorem and/or layer potentials [4]. Several versions of the BIM exist depending on the choice of basis functions and discretization [17,6,13].

A hybrid boundary method unifying BIM and PWDM has been developed in [6]. This method, called the gauge freedom method (GFM), has as its main advantage the choice of a regular kernel in the integral equation.

BIM approaches are fundamental tools in both the numerical solution and in the theoretical analysis. Uniqueness and existence theorems are often much easier established in this way.

Another major advantage of the integral equation representation for external problems is that these ensure that the Sommerfeld radiation condition is automatically satisfied exactly. While considerable progress has been made in developing the so-called perfectly matched layers to imitate the properties of the far-field, these are relatively difficult to implement.

Despite these advantages the integral equation approaches have some minor disadvantages. The first is that their formulation is relatively more complex mathematically. However, this need not be an obstacle to their understanding and implementation, since there are many relatively clear expositions of the integral equation approaches. A second disadvantage of the integral equation approach is that it leads to linear systems with dense matrices. For large sizes, these dense matrices are relatively expensive to perform computations with. Many modern calculations require characterization of the scattering off complex shaped objects, where large matrices arise. The fast multipole methods (FMM) [23] allow computation of the product of a vector with a dense matrix of the kind that arises upon discretization of the integral equation to be done extremely rapidly, and go a long way towards alleviating this disadvantage.

The most crucial issue and major problem in BIM implementations is the evaluation of singular and hypersingular integrals involved in the integral equations. These integrals contribute to the dominant (diagonal and near diagonal) terms of the discretized boundary element matrices. The treatment of singular and hypersingular integrals has been a subject of investigation for the development of BIM in the past decades, and many techniques have been proposed so far. We will make no attempt to review these many contributions (see, e.g., [22] and the references therein), as this goes beyond the scope of this paper. These methods include analytical integration if possible [22,18], approximation by equations with smooth kernels [7,25] and subtraction of the singularity [2].

In this paper we consider a new approach where we can compute the singular and hypersingular parts of the integrals involved in BIM by a simple use of Green's theorem and particular solutions of the Helmholtz equations. We show computational results for 2D domains, but the method can be easily extended to the three-dimensional (3D) case. The numerical results will be compared to the very efficient method in [18,5, Chapter 3.5], where analytical computation of the diagonal elements with a Nyström discretization were performed. We will demonstrate that our method has exponential convergence, and is much easier to implement, especially for the hypersingular kernel, compared to the previously mentioned methods.

The paper is organized as follows. In Section 2 we recall the boundary integrals and discuss briefly the derivation of boundary integral equations. In Section 3 we implement the numerical algorithm and discuss few examples. Finally, in Section 4, we summarize the results.

2. Boundary integral formulation

First, let us introduce the boundary integral operators. We denote the fundamental solution of Eq. (1.1) (the free-space source) by

$$\Phi(\mathbf{x},\mathbf{y}) = -\frac{i}{2}H_0^{(1)}(k|\mathbf{x}-\mathbf{y}|),$$

where $H_0^{(1)}$ is the Hankel function of order zero and the first kind.

For $\phi,\psi \in C(\Gamma)$, define the single and double layer potentials

$$S\phi(\mathbf{x}) = \int_\Gamma \Phi(\mathbf{x},\mathbf{y})\phi(\mathbf{y})\,ds(\mathbf{y}), \quad \mathbf{x}\in\mathbf{R}^2\backslash\Gamma \tag{2.1}$$

and

$$D\psi(\mathbf{x}) = \int_\Gamma \frac{\partial}{\partial\nu(\mathbf{y})}\Phi(\mathbf{x},\mathbf{y})\psi(\mathbf{y})\,ds(\mathbf{y}), \quad \mathbf{x}\in\mathbf{R}^2\backslash\Gamma \tag{2.2}$$

with densities ϕ and ψ, respectively. Their normal derivatives are given by

$$M\phi(\mathbf{x}) = \frac{\partial}{\partial\nu(\mathbf{x})}S\phi(\mathbf{x}) \quad \text{and} \quad N\psi(\mathbf{x}) = \frac{\partial}{\partial\nu(\mathbf{x})}D\psi(\mathbf{x}). \tag{2.3}$$

It is known (cf. [4, Sections 2.4 and 2.5]) that the above defined potentials are analytic in $\mathbf{R}^2\backslash\Gamma$ and when $\mathbf{x}$ approaches Γ, S and N are continuous, whereas D and M exhibit jumps. In particular, on Γ,

$$S\to\hat{S}, \quad N\to\hat{N}, \quad D\to\mp I+\hat{D} \quad \text{and} \quad M\to\pm I+\hat{M}, \tag{2.4}$$

where the upper (resp. lower) sign corresponds to the limit when $\mathbf{x}$ approaches Γ from outside (resp. inside) and I is the identity operator. The compact operators $\hat{S},\hat{M},\hat{D}: C(\Gamma)\to C(\Gamma)$ are given, on Γ, by

$$\hat{S}\phi(\mathbf{x}) = \int_\Gamma \Phi(\mathbf{x},\mathbf{y})\phi(\mathbf{y})\,ds(\mathbf{y}), \quad \mathbf{x}\in\Gamma,$$

$$\hat{M}\phi(\mathbf{x}) = \int_\Gamma \frac{\partial}{\partial\nu(\mathbf{x})}\Phi(\mathbf{x},\mathbf{y})\phi(\mathbf{y})\,ds(\mathbf{y}), \quad \mathbf{x}\in\Gamma,$$

$$\hat{D}\psi(\mathbf{x}) = \int_\Gamma \frac{\partial}{\partial\nu(\mathbf{y})}\Phi(\mathbf{x},\mathbf{y})\psi(\mathbf{y})\,ds(\mathbf{y}), \quad \mathbf{x}\in\Gamma$$

and the unbounded operator $\hat{N}: \Upsilon(\Gamma) \to C(\Gamma)$ is given, on Γ, by

$$\hat{N}\psi(\mathbf{x}) = \frac{\partial}{\partial \nu(\mathbf{x})} \int_\Gamma \frac{\partial}{\partial \nu(\mathbf{y})} \Phi(\mathbf{x},\mathbf{y})\psi(\mathbf{y})\, ds(\mathbf{y}), \quad \mathbf{x} \in \Gamma.$$

Here $\Upsilon(\Gamma)$ is the linear space of all continuous functions ψ with the property that the double layer potential with density ψ has continuous normal derivatives on both sides of Γ. It can be shown that, for two different wave numbers $\tilde{k}$ and k, $\hat{N} - \hat{N}_{\tilde{k}}$ is a compact operator in $C(\Gamma)$. The operator $\hat{N}_{\tilde{k}}$ is the same as $\hat{N}$ with the wave number k replaced by $\tilde{k}$. We refer to [4, Section 2.7] for details and proof of compactness for the above operators.

Next, we derive Green's representation formula. Multiplying the Helmholtz equation by Φ and integrating over Γ, using the Sommerfel radiation condition, leads to

$$\begin{cases} 2u^s(\mathbf{x}) = S\dfrac{\partial}{\partial \nu}u(\mathbf{x}) - Du(\mathbf{x}), & \mathbf{x} \in \mathbf{R}^2 \backslash \Omega, \\ -2u^{inc}(\mathbf{x}) = S\dfrac{\partial}{\partial \nu}u(\mathbf{x}) - Du(\mathbf{x}), & \mathbf{x} \in \Omega. \end{cases} \tag{2.5}$$

Indeed, for $\mathbf{x} \in \mathbf{R}^2 \backslash \Omega$, from Theorem 3.1 in [4], we have

$$0 = S\frac{\partial}{\partial \nu}u^{inc}(\mathbf{x}) - Du^{inc}(\mathbf{x})$$

and by Theorem 3.2 in [4] we have

$$2u^s(\mathbf{x}) = S\frac{\partial}{\partial \nu}u^s(\mathbf{x}) - Du^s(\mathbf{x}).$$

By adding the previous two equations, using $u = u^s + u^{inc}$, we obtain the first equation in (2.5). Similarly, for $\mathbf{x} \in \Omega$, from Theorem 3.1 in [4], we have

$$-2u^{inc}(\mathbf{x}) = S\frac{\partial}{\partial \nu}u^{inc}(\mathbf{x}) - Du^{inc}(\mathbf{x})$$

and by Theorem 3.2 in [4] we have

$$0 = S\frac{\partial}{\partial \nu}u^s(\mathbf{x}) - Du^s(\mathbf{x}).$$

By adding the previous two equations, using $u = u^s + u^{inc}$, we obtain the second equation in (2.5).

From the second equation in (2.5), and (2.4) we have

$$\begin{cases} -2u^{inc} = \hat{S}\dfrac{\partial}{\partial \nu}u - (I + \hat{D})u \\ -2\dfrac{\partial}{\partial \nu}u^{inc} = (\hat{M} - I)\dfrac{\partial}{\partial \nu}u - \hat{N}u \end{cases} \quad \text{on } \Gamma. \tag{2.6}$$

From the previous system we see that the solution of the Dirichlet problem can be found by solving

$$-2u^{inc} = \hat{S}\sigma \quad \text{or} \quad -2\frac{\partial}{\partial \nu}u^{inc} = (\hat{M} - I)\sigma \tag{2.7}$$

on Γ, where $\sigma = (\partial/\partial \nu)u$. Similarly the solution of the Neumann problem can be obtained by solving

$$2\frac{\partial}{\partial \nu}u^{inc} = \hat{N}\tilde{\sigma} \quad \text{or} \quad 2u^{inc} = (I + \hat{D})\tilde{\sigma} \tag{2.8}$$

on Γ, where $\hat{\sigma} = u$.

To solve the transmission problem we present the field inside Ω by a single layer potential $u_i = S_i\hat{\sigma}$ with unknown density function $\hat{\sigma}$, where S_i is the same as S, with k replaced by k_i. By (2.4) we have

$$\begin{cases} u_i = \hat{S}_i\hat{\sigma} \\ \dfrac{\partial}{\partial \nu}u_i = (\hat{M}_i - I)\hat{\sigma} \end{cases} \quad \text{on } \Gamma.$$

From the previous system and (2.6) we see that the solution of the transmission problem can be obtained by solving

$$-2u^{inc} = \hat{A}\hat{\sigma} \quad \text{or} \quad -2\frac{\partial}{\partial \nu}u^{inc} = \hat{B}\hat{\sigma} \tag{2.9}$$

on Γ, where

$$\hat{A} = \rho\hat{S}(\hat{M}_i - I) - (I + \hat{D})\hat{S}_i \quad \text{and} \quad \hat{B} = \rho(\hat{M} - I)(\hat{M}_i - I) - \hat{N}\hat{S}_i.$$

Once we solve the equations in (2.7), (2.8) and (2.9) we find σ, $\hat{\sigma}$ and $\tilde{\sigma}$, respectively, and recover u^s from (2.5). In conclusion we see that, for each boundary value problem, we have two different integral equations that we can solve in order to find the solution of the considered problem. Unfortunately, there are irregular wave numbers, the so-called interior eigenvalues, for which these equations are not uniquely solvable (cf. [4, Section 3.9]). Many methods have been proposed in the literature to overcome this problem (cf. [25] for review).

To get unique solutions for all values of the wave number k we can consider the linear combination of the two equations (cf. [1,16,4]), i.e., for $\eta \neq 0$, we have, for each case the following equation:

1. Dirichlet:

$$-2u^{inc} + 2i\eta\frac{\partial}{\partial \nu}u^{inc} = (\hat{S} - i\eta(\hat{M} - I))\sigma \quad \text{on } \Gamma. \tag{2.10}$$

2. Neumann:

$$2u^{inc} - 2i\eta\frac{\partial}{\partial \nu}u^{inc} = (I + \hat{D} - i\eta\hat{N})\tilde{\sigma} \quad \text{on } \Gamma. \tag{2.11}$$

3. Transmission:

$$-2u^{inc} + 2i\eta\frac{\partial}{\partial \nu}u^{inc} = (\hat{A} - i\eta\hat{B})\hat{\sigma} \quad \text{on } \Gamma. \tag{2.12}$$

Another alternative is to use a combination of single and double layer potentials (cf. [21,19,16,4]). The solution is sought in the form

$$u^s(\mathbf{x}) = (D - i\eta S)\phi(\mathbf{x}), \quad \mathbf{x} \in \mathbf{R}^2 \backslash \Omega \tag{2.13}$$

for an unknown function ϕ, where $\eta \neq 0$ is a real number. In this case we will have the following equations.

1. Dirichlet:

$$u^{inc} = (\hat{D} - I - i\eta\hat{S})\phi \quad \text{on } \Gamma. \tag{2.14}$$

2. Neumann:

$$\frac{\partial}{\partial \nu}u^{inc} = (\hat{N} - i\eta(\hat{M} + I))\phi \quad \text{on } \Gamma. \tag{2.15}$$

3. Transmission: In this case we represent the field inside as a combination of single and double layer, as well, i.e., $u_i = (S_i - i\xi D_i)\hat{\sigma}$, $\xi \neq 0$, and we obtain

$$\begin{cases} (\hat{S}_i - i\xi(I + \hat{D}_i))\hat{\sigma} - u^{inc} = (\hat{D} - I - i\eta\hat{S})\phi \\ (\hat{M}_i - I - i\xi N_i)\hat{\sigma} - \dfrac{\partial}{\partial \nu}u^{inc} = (\hat{N} - i\eta(I + \hat{M}))\phi \end{cases} \quad \text{on } \Gamma. \tag{2.16}$$

Since we have two alternatives for obtaining a unique solution for the integral equations resulting from the three problems, we choose the problem with the least computational effort. Accordingly we consider (2.14) for the Dirichlet problem, (2.15) for the Neumann problem and (2.12) for the Transmission problem. Thus, in the sequel we will consider the following problem: find $\phi \in C(\Gamma)$ such that

$$\hat{C}\phi = f \quad \text{on } \Gamma, \tag{2.17}$$

where

$$\hat{C} = \begin{cases} ((\hat{D} - I) - i\eta\hat{S}) & \text{Dirichlet integral equation,} \\ (\hat{N} - i\eta(\hat{M} + I)) & \text{Neumann integral equation,} \\ (\hat{A} - i\eta\hat{B}) & \text{Transmission integral equation,} \end{cases}$$

and

$$f=\begin{cases} u^{inc} & \text{Dirichlet integral equation,}\\ \frac{\partial}{\partial \nu}u^{inc} & \text{Neumann integral equation,}\\ -2u^{inc}+2i\eta\frac{\partial}{\partial \nu}u^{inc} & \text{Transmission integral equation.}\end{cases}$$

3. The numerical method and results

For numerical solutions of integral equations of the second kind, there are roughly three methods: the Nyström method, the collocation method and the Galerkin method. In the case of 1D integral equations, the Nyström method has proved to be more practical than the other methods [18]. It is stable, whereas the other methods are unstable for a poor choice of the basis. It requires the least computational effort since, for evaluation of the resulting linear system, only an evaluation of the kernel function is needed, whereas in the other two methods the matrix elements are simple or double integrals demanding numerical quadratures.

In the sequel we assume that the incident field u^{inc} is a plane wave, i.e., $u^{inc}(\mathbf{x})=e^{ik\mathbf{x}\cdot\mathbf{d}}$, where $\mathbf{d}=[\cos(\alpha),\sin(\alpha)]$, and α describes the angle of the propagation.

3.1. Parametrization and discretization

The boundary Γ is assumed to possess regular analytic and 2π-periodic representation of the form

$$\mathbf{x}(t)=[\mathbf{x}_1(t),\mathbf{x}_2(t)],\quad 0\leqslant t\leqslant 2\pi, \tag{3.1}$$

in counterclockwise orientation, such that, the unit outward normal $\nu(\mathbf{x})$ is written as

$$\nu(\mathbf{x}(t))=\frac{1}{|\mathbf{x}'(t)|}\mu(t), \tag{3.2}$$

where $\mu(t)=[\mathbf{x}_2'(t),-\mathbf{x}_1'(t)]$. Nyström's method replaces the integrals by integrals of the trigonometric interpolation polynomials of the integrands. In particular, for $J\in\mathbf{N}$ and $t_j=\pi j/J$, $j=0,\ldots,2J-1$, the integrals of the form $\int_0^{2\pi}g(\tau)\,d\tau$ are approximated such that

$$\int_0^{2\pi}g(\tau)\,d\tau\approx\frac{\pi}{J}\sum_{j=0}^{2J-1}g(t_j). \tag{3.3}$$

3.2. Computation of the discretized terms for $\hat{S}$, $\hat{D}$, $\hat{M}$ and $\hat{N}$

We write $\hat{S}$, $\hat{D}$, $\hat{M}$ and $\hat{N}$ in the form

$$\hat{U}\phi(\mathbf{x})=\int_\Gamma U(\mathbf{x},\mathbf{y})\phi(\mathbf{y})\,ds(\mathbf{y}), \tag{3.4}$$

where the kernel U is given as

$$U(\mathbf{x},\mathbf{y})=-\frac{i}{2}\times\begin{cases} H_0^{(1)}(k|\mathbf{x}-\mathbf{y}|) & \text{when } \hat{U}=\hat{S},\\ \frac{\partial}{\partial\nu(\mathbf{y})}H_0^{(1)}(k|\mathbf{x}-\mathbf{y}|) & \text{when } \hat{U}=\hat{D},\\ \frac{\partial}{\partial\nu(\mathbf{x})}H_0^{(1)}(k|\mathbf{x}-\mathbf{y}|) & \text{when } \hat{U}=\hat{M},\\ \frac{\partial}{\partial\nu(\mathbf{x})}\left(\frac{\partial}{\partial\nu(\mathbf{y})}H_0^{(1)}(k|\mathbf{x}-\mathbf{y}|)\right) & \text{when } \hat{U}=\hat{N}.\end{cases}$$

Replacing $\mathbf{x}$ by $\mathbf{x}(t)$ and $\mathbf{y}$ by $\mathbf{x}(\tau)$ we use the notation $U(t,\tau)=U(\mathbf{x}(t),\mathbf{x}(\tau))$, $\phi(t)=\phi(\mathbf{x}(t))$ and the integral in (3.4) is written as

$$\hat{U}\phi(t)=\int_0^{2\pi}U(t,\tau)\phi(\tau)|x'(\tau)|\,d\tau. \tag{3.5}$$

Next, we may write $\hat{U}\phi$ in the form

$$\hat{U}\phi(t)=\int_0^{2\pi}U(t,\tau)|x'(\tau)|(\phi(\tau)-\phi(t))\,d\tau+\phi(t)\int_0^{2\pi}U(t,\tau)|x'(\tau)|\,d\tau. \tag{3.6}$$

Using the quadrature rule in (3.3) we may replace the right-hand side of (3.6) by an approximation for an approximate function $\tilde{\phi}$:

$$\frac{\pi}{M}\sum_{j=0}^{2J-1}U(t,\tau_j)|x'(\tau_j)|(\tilde{\phi}(\tau_j)-\tilde{\phi}(t))+\tilde{\phi}(t)Q(t), \tag{3.7}$$

where

$$Q(t)=\int_0^{2\pi}U(t,\tau)|x'(\tau)|\,d\tau.$$

If we replace t by t_i, $i=0,1,\ldots,2J-1$, in (3.7) we obtain an approximation of $\hat{U}\phi$ which may be written in matrix notation as $\mathbf{P}\tilde{\phi}$, where $\mathbf{P}=\mathbf{U}-\mathbf{V}$, $\mathbf{U}=[u_{ij}]$,

$$u_{ij}=\frac{\pi}{M}U(t_i,\tau_j)|x'(\tau_j)|,$$

$\mathbf{V}$ is a diagonal matrix with entries

$$v_{ii}=\frac{\pi}{M}\sum_{j=0}^{2J-1}U(t_i,\tau_j)|x'(\tau_j)|-Q(t_i),$$

and $\tilde{\phi}$ is a vector of entries $\tilde{\phi}_i=\phi(t_i)$, $i=0,\ldots,2J-1$.

We see that the off-diagonal terms of $\mathbf{P}$ are easily computed in u_{ij} and the problem that remains is that of finding an (analytic or numerical) approximation for the diagonal terms. In [5, Section 3.5; 18] the kernel U is divided into a combination of kernels where a special quadrature (with the above discretization) was used and the terms $U(t,t)$ are computed analytically. We will refer to this method as the Kress–Nystöm method (KNM). Here we choose an alternative route. In particular, we use the above discretization for the computation of the off-diagonal elements and Green's identity to compute the diagonal elements. We will call this procedure Green's identity method (GIM) and compare our results below with the KNM. Next we show how to implement the GIM.

We notice that, for any direction $\mathbf{d}$, $u^{inc}(\mathbf{x})=e^{ik\mathbf{x}\cdot\mathbf{d}}$ is a solution of the Helmholtz equation in Ω and we can replace u by u^{inc} in the second equation of system (2.5) (cf. [4, Theorem 3.1]). We exploit this observation to compute an approximation to the terms $U(t,t)$.

Let us take two incident fields u_l^{inc} with directions $\mathbf{d}_l$, $l=1,2$. From the first equation in (2.6) we get, for $l=1,2$,

$$-2u_l^{inc}=\hat{S}\frac{\partial}{\partial\nu}u_l^{inc}-(I+\hat{D})u_l^{inc}\quad\text{on }\Gamma. \tag{3.8}$$

Now, using the Nyström discretization method described above, we obtain from (3.8), for $i=0,1,\ldots,2J-1$,

$$-2u_l^{inc,i}\approx\left[\sum_{j=0,j\neq i}^{2J-1}s_{ij}+s_{ii}\right]\frac{\partial}{\partial\nu}u_l^{inc,i}-\left[1+\sum_{j=0,j\neq i}^{2J-1}d_{ij}+d_{ii}\right]u_l^{inc,i},\quad l=1,2,$$

where $u_l^{inc,i}=u_l^{inc}(t_i)$. Now, for every $i=0,\ldots,2J-1$ we can use this system to compute d_{ii} and s_{ii} since s_{ij} and d_{ij} are known for $i\neq j$. From the definition of the derivative of the single layer M and the double layer D it is clear that the diagonal terms of $\mathbf{D}$ (the matrix obtained from $\hat{D}$) and the diagonal term of $\mathbf{M}$ (the matrix obtained from $\hat{M}$) have the following relation: $m_{ii}=-d_{ii}$, for $i=0,\ldots,2J-1$. We finally obtain the diagonal term n_{ii}, $i=0,\ldots,2J-1$, of $\mathbf{N}$ (the matrix obtained from $\hat{N}$) from the second equation in (2.6) using one incident field.

Now, having computed an approximation for $\hat{S}$, $\hat{D}$, $\hat{M}$ and $\hat{N}$, we may write the problem in (2.17) in the matrix form

$$\mathbf{C}\tilde{\phi}=\mathbf{f}. \tag{3.9}$$

We solve this problem by the two-grid method [18]. The solution can be quickly obtained by using the FMM for the matrix–vector multiplications [10].

Remark. It is clear that this way of computing the diagonal elements of the matrices resulting from the layer potentials and their derivatives is easily implemented in the Gallerkin or collocation methods. Moreover, since Green's identities are valid in the 3D problem, we do not expect any difficulty for extending the method to that case.

3.3. Numerical examples and discussion

In the examples below, for given domains, we compute the diagonal elements for the single layer, the double layer and their derivatives at various frequencies (wave numbers). We also calculate the far field patterns for various frequencies and angles. In all our examples we will use $k_i = 2$ for the transmission problem.

Now, let us introduce the far field pattern and its numerical approximation. It is well known that u has the following asymptotic behavior:

$$u(\mathbf{x}) = \frac{e^{ik|\mathbf{x}|}}{\sqrt{|\mathbf{x}|}}\left\{u_\infty(\hat{\mathbf{x}}) + O\left(\frac{1}{|\mathbf{x}|}\right)\right\} \quad |\mathbf{x}| \to \infty \tag{3.10}$$

uniformly in all directions $\hat{\mathbf{x}} := \mathbf{x}/|\mathbf{x}|$ (cf. [5, Theorem 2.5]) where u_∞ is known as the far field pattern.

We wish to compute an approximation u_∞^{app} of the far field pattern u_∞. Using (3.10) and the asymptotics of Hankel functions (cf. [5, p. 65]) in (2.13), we obtain

$$u_\infty(\hat{\mathbf{x}}) = \frac{e^{-i(i/4)}}{\sqrt{8\pi k}}\int_\Gamma (kv(\mathbf{y})\cdot\hat{\mathbf{x}} + \eta)e^{-ik\hat{\mathbf{x}}\cdot\mathbf{y}}\phi(\mathbf{y})\,ds(\mathbf{y}), \tag{3.11}$$

which is the far field pattern of the Dirichlet (resp. Neumann) problem, and ϕ is the solution of the Dirichlet (resp. Neumann) integral equation. Similarly, using the asymptotics of Hankel functions in the first equation of (2.5), we obtain the far field pattern for the transmission problem

$$u_\infty^T(\hat{\mathbf{x}}) = \frac{e^{-i(i/4)}}{\sqrt{8\pi k}}\int_\Gamma (kv(\mathbf{y})\cdot\hat{\mathbf{x}}\phi_1(\mathbf{y}) + \eta\phi_2(\mathbf{y}))e^{-ik\hat{\mathbf{x}}\cdot\mathbf{y}}\,ds(\mathbf{y}), \tag{3.12}$$

where $\phi_1 = \hat{S}_i\phi$, $\phi_2 = (\hat{D}_i - I)\phi$, and ϕ is the solution of the transmission integral equation.

We use (3.1)–(3.3) to have a discrete form of (3.11) and (3.12)

$$u_\infty^{\text{app}}(\hat{\mathbf{x}}) = \frac{e^{-i(i/4)}}{\sqrt{8\pi k}}\sum_{j=0}^{2J-1}(k\mu_j\cdot\hat{\mathbf{x}} + \eta)e^{-ik\hat{\mathbf{x}}\cdot\mathbf{x}_j}\tilde{\phi}_j \tag{3.13}$$

and

$$u_\infty^{T,\text{app}}(\hat{\mathbf{x}}) = \frac{e^{-i(i/4)}}{\sqrt{8\pi k}}\sum_{j=0}^{2J-1}(k\mu_j\cdot\hat{\mathbf{x}}\tilde{\phi}_{1,j} - \tilde{\phi}_{2,j})e^{-ik\hat{\mathbf{x}}\cdot\mathbf{x}_j}$$

where $\tilde{\phi}_1 = \hat{S}_i\tilde{\phi}$, $\tilde{\phi}_2 = (\hat{D}_i - I)\tilde{\phi}$, and $\tilde{\phi}$ is a solution of (3.9).

Example 1 (*A circular domain*). Here we assume a circular cross-section of radius a i.e.,

$$x_1 = a\cos(t), \quad x_2 = a\sin(t).$$

In this case we can compute the solution analytically using the Fourier expansion of Bessel functions (cf. [8]). First, we compare the results for GIM and KNM for the diagonal elements. In particular, we plot L_2, the l^2 norm of a vector filled with the diagonal elements of $\hat{S}$, $\hat{D}$, $\hat{M}$ or $\hat{N}$, against J, the Nyström points. In Fig. 1 we have the results for the single layer potential for two different wave numbers. We see that for large J the two methods give very similar results, but for larger wave numbers we need more grid points to get the same values for L_2 in the two methods. In Fig. 2 we have the case of the double layer or the derivative of the single layer since both potentials lead to the same values of L_2. In this case the analytical result obtained from KNM is independent of the wave number k, and only GIM varies with k. We see a fast convergence of L_2, and, as for the single layer, we need more grid points for larger wave numbers in order for GIM to get the same result as KNM. Finally, we show the result of the derivative of the double layer in Fig. 3. In contrast to the other two potentials we have, due to its hypersingular nature, divergence and the same results are obtained only for lower values of J.

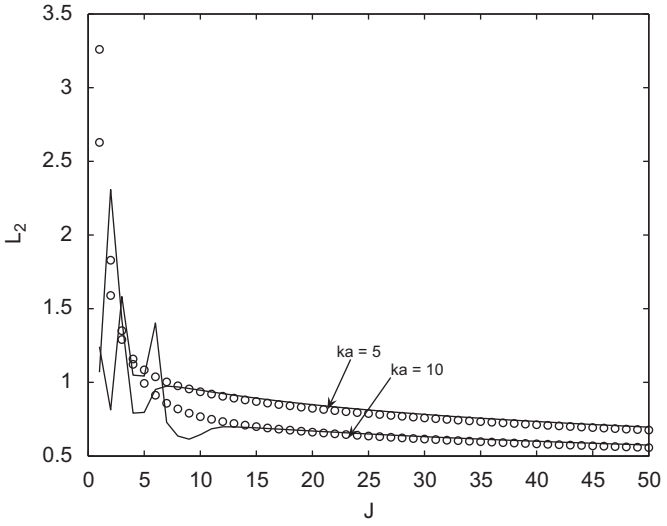

Fig. 1. Here we plot the l^2 norm (L_2) of the vector filled with the diagonal elements of $\hat{S}$ against the grid points J using KNM ('○') and GIM (solid line) for different values of ka.

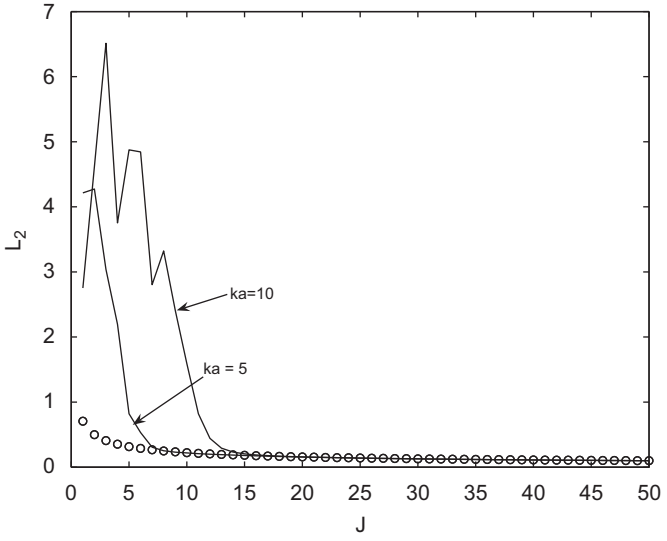

Fig. 2. Here we plot the l^2 norm (L_2) of the vector filled with the diagonal elements of $\hat{M}$ and $\hat{D}$ against the grid points J using KNM ('○') and GIM (solid line) for different values of ka.

Next, we compute the far field pattern. First, for fixed incident and observation angles, we compute the far field for the three problems using the analytical result and the two methods at different grid points. The results are reported in Table 1 for $ka = 4$, and in Table 2 for $ka = 10$. The two methods give very similar

results and converge to the exact solution. For larger values of ka we need larger value of J.

We should point out that like KNM, GIM (which is much easier to implement, especially for the hypersingular kernel) has exponential convergence. Moreover the evaluation of the sum in the computation of the diagonal elements for GIM can be done faster by using FMM [10]. In Fig. 4 we plot the absolute value of the far field, for the three problems, against the incident angle at $J = 30$ and $ka = 4$. We see a very good match for the two methods. The same observation is seen for larger k in Figs. 5, 6 and 7 for Dirichlet, transmission and Neumann problems, respectively. For these figures we used $ka = 15$ and $J = 40$.

Example 2 (*A rounded rectangle*). Here we consider a convex cross-section given in Fig. 8. It has the following form:

$$(ax_1)^{10} + \left(a\frac{2}{3}x_2\right)^{10} = 1.$$

We can use the same parametrization as described above and compute analytically the partial derivatives (up to the third order) needed in our computations. We cannot, for this example, have

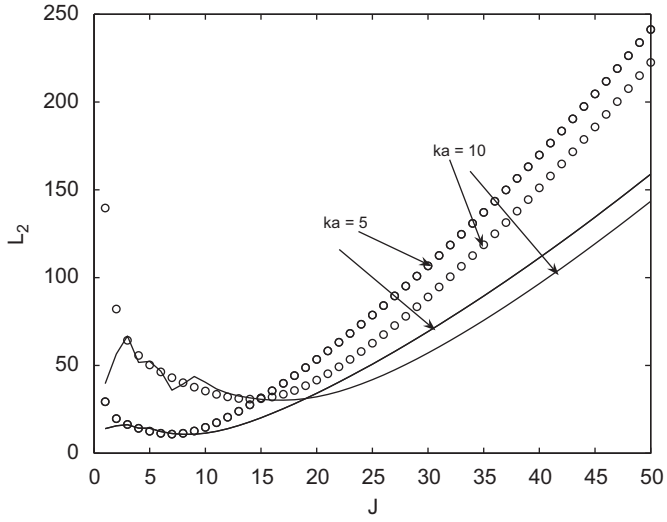

Fig. 3. Here we plot the l^2 norm (L_2) of the vector filled with the diagonal elements of $\hat{N}$ against the grid points J using KNM ('∘') and GIM (solid line) for different values of ka.

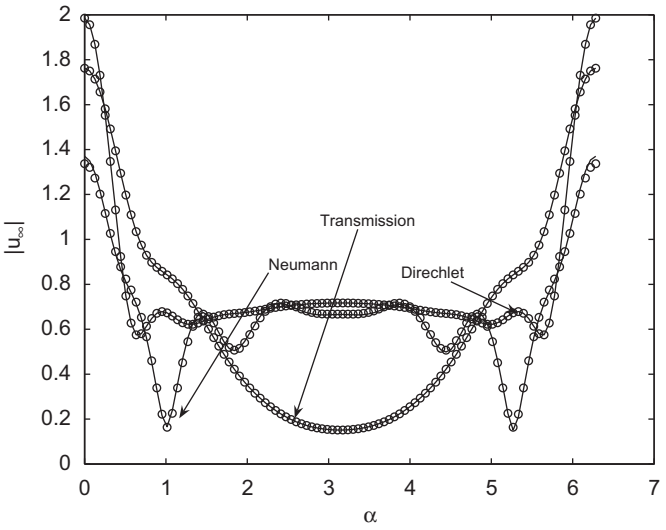

Fig. 4. Here we plot $|u_\infty|$ against the angle α using KNM ('∘') and GIM (solid line) for the three problems in Example 1, for $ka = 4$.

Table 1
The numerical results using GIM, KNM and the analytical (exact) solution for $ka = 4$.

Wave number	Exact	Nyström points	KNM	GIM
Dirichlet	$-1.7385 + 0.9586i$	$J = 10$	$-1.7384 + 0.9587i$	$-1.7269 + 0.9539i$
		$J = 30$	$-1.7385 + 0.9586i$	$-1.7385 + 0.9586i$
Neumann	$-0.6373 + 1.1755i$	$J = 10$	$-0.6367 + 1.1763i$	$-0.6377 + 1.1771i$
		$J = 30$	$-0.6373 + 1.1755i$	$-0.6374 + 1.1756i$
Transmission	$-1.5044 + 0.9171i$	$J = 10$	$-1.5051 + 0.9171i$	$-1.4970 + 0.9254i$
		$J = 30$	$-1.5044 + 0.9171i$	$-1.5042 + 0.9174i$

Table 2
The numerical results using GIM, KNM and the analytical (exact) solution for $ka = 10$.

Wave number	Exact	Nyström points	KNM	GIM
Dirichlet	$-2.3077 + 1.6412i$	$J = 10$	$-1.8687 + 1.3030i$	$-1.1514 + 1.0308i$
		$J = 20$	$-2.3068 + 1.6412i$	$-2.2851 + 1.6120i$
		$J = 30$	$-2.3077 + 1.6412i$	$-2.3070 + 1.6403i$
Neumann	$-1.3456 + 1.8598i$	$J = 10$	$-1.7780 + 1.7008i$	$-1.7898 + 1.7042i$
		$J = 20$	$-1.3454 + 1.8610i$	$-1.3457 + 1.8615i$
		$J = 30$	$-1.3456 + 1.8598i$	$-1.3456 + 1.8599i$
Transmission	$-2.1447 + 1.5517i$	$J = 10$	$-1.9646 + 1.1395i$	$-2.6156 + 0.6762i$
		$J = 20$	$-2.1446 + 1.5518i$	$-2.1560 + 1.5736i$
		$J = 30$	$-2.1447 + 1.5517i$	$-2.1449 + 1.5523i$

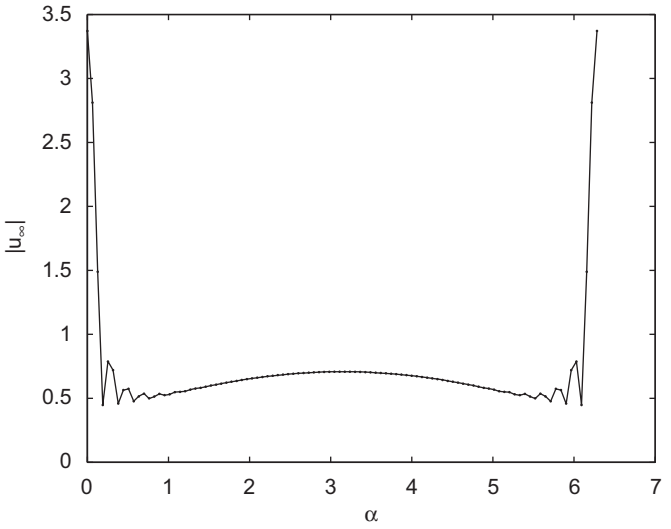

Fig. 5. Here we plot $|u_\infty|$ against the angle α using KNM ('·') and GIM (solid line) for the Dirichlet problem in Example 1, for $ka = 15$.

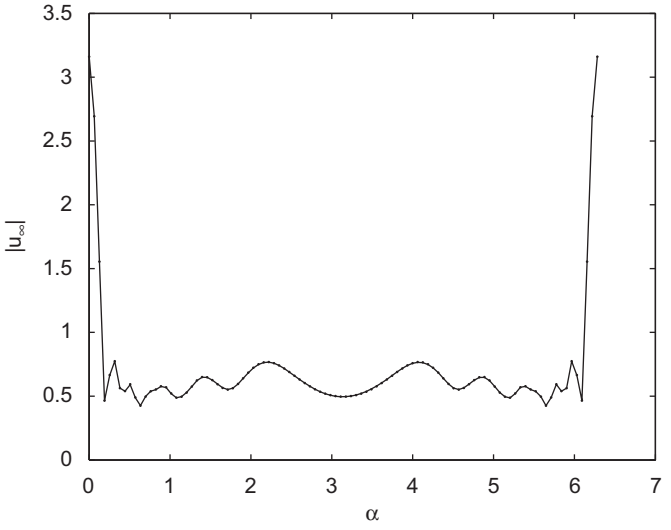

Fig. 6. Here we plot $|u_\infty|$ against the angle α using KNM ('·') and GIM (solid line) for the transmission problem in Example 1, for $ka = 15$.

analytical expressions of the far field. We have computed the far field for the three problems, using GIM and KNM, and plot the absolute values against the incident angle for $ka = 7$ and $J = 40$. The result is in Fig. 9. We see for this example as well that the two methods give the same results.

Example 3 (*A non-convex domain*). Finally we consider the cross-section given in Fig. 10. It has the following parametrization:

$$x_1 = a\cos(t) + 0.65a\cos(2t) - 0.65a, \quad x_2 = 1.5a\sin(t).$$

In this case it is much easier to compute analytically the partial derivatives than in Example 2. Like in the previous example we plot the absolute value of the far field pattern against the incident angle for the three problems using $ka = 7$ and $J = 40$. The result is in Fig. 11. As for the previous examples we have a very good match for the two methods.

We would like to mention that for this example as well as for the rounded rectangle we have computed the l^2 norm for the

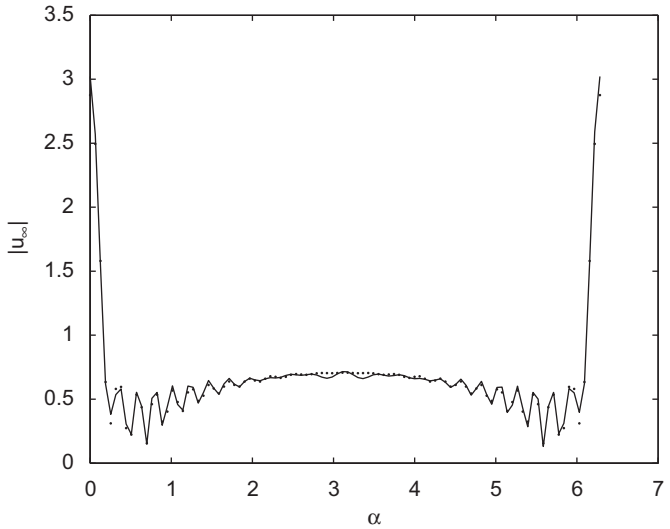

Fig. 7. Here we plot $|u_\infty|$ against the angle α using KNM ('·') and GIM (solid line) for the Neumann problem in Example 1, for $ka = 15$.

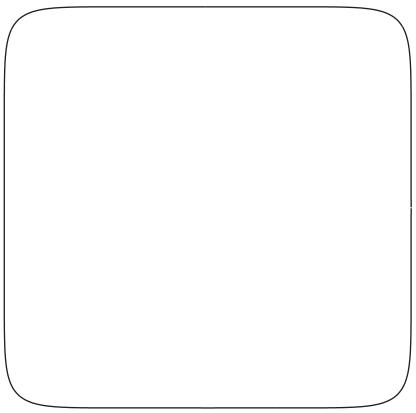

Fig. 8. Cross-section for Example 2.

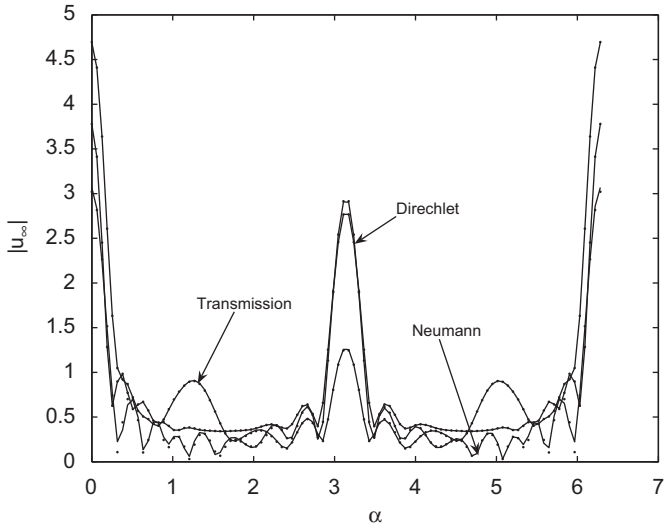

Fig. 9. Here we plot $|u_\infty|$ against the angle α using KNM ('·') and GIM (solid line) for the three problems in Example 2, for $ka = 7$.

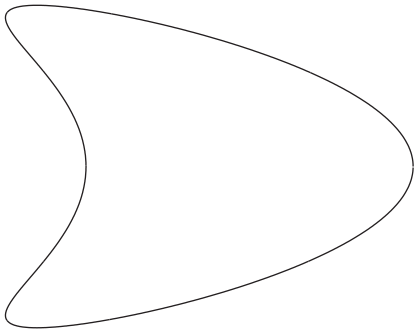

Fig. 10. Cross-section for Example 3.

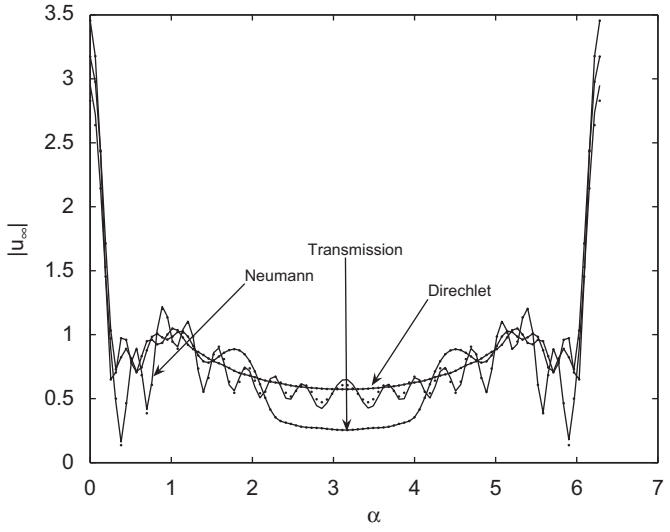

Fig. 11. Here we plot $|u_\infty|$ against the angle α using KNM ('·') and GIM (solid line) for the three problems in Example 3, for $ka = 7$.

diagonal elements at various values of J and we have seen the same scenario as for Example 1 (cf. Figs. 1–3).

4. Conclusion

In this paper we have shown a method for computing singular and hypersingular integrals involved in a large class of boundary value problems. The method, which is based on Green's theorem for calculating the diagonal elements of the resulting discretized matrix, is easy to implement numerically. Here we used the Nyström discretization and compared our results with a method due to Kress [18]. Our method shows fast convergence and the results are similar to those obtained by KNM. Our computation can be made much quicker using FMM and multigrid techniques. In the future we would compute 3D problems from one obstacle to thousands (multiple scattering) using GIM and very fast matrix–vector multiplication algorithms.

References

[1] Burton AJ, Miller GF. The application of integral equation methods to the numerical solution of some exterior boundary-value problems. Proc R Soc London A 1971;323:201–10.
[2] Chen Ke. Efficient iterative solution of linear systems from discretizing singular integral equations. Electron Trans Numer Anal 1994;2:76–91.
[4] Colton D, Kress R. Integral equation methods in scattering theory. New York: Wiley; 1983.
[5] Colton D, Kress R. Inverse acoustic and electromagnetic scattering theory. second ed. Berlin: Springer; 1997.
[6] Cohen D, Lepore N, Heller EJ. Consolidating boundary methods for finding the eigenstates of billiards. J Phys A Math Gen 2004;37:2139–61 PII: S0305-4470(04)69126-8.
[7] Duduchava R, Prössdorf S. On the approximation of singular integral equations by equations with smooth kernels. Integral Equations and Operator Theory 1995;21:223–37.
[8] Felbacq D, Tayeb G, Maystre D. Scattering by a random set of parallel cylinders. J Opt Soc Am A 1994;11(9):2526–38.
[10] N.A. Gumerov, R. Duraiswami, A broadband fast multipole accelerated boundary element method for the 3D Helmholtz equation. J Acoust Soc Am 2009;125(1):191–205.
[11] Gutkin B. Can billiard eigenstates be approximated by superpositions of plane waves? J Phys A Math Gen 2003;36:8603–22.
[12] Heller EJ. In: Giannoni M-J, Voros A, Zinn-Justin J, editors. Chaos and quantum systems. Amsterdam: Elsevier; 1991. p. 548.
[13] Kaufman DL, Kosztin I, Schulten K. Expansion method for stationary states of quantum billiards. Am J Phys 1999;67.
[15] Kirsch A, Monk P. Convergence analysis of a coupled finite element and spectral method in acoustic scattering. IMA J Numer Anal 1990;9:425–47.
[16] Kleinman RE, Martin PA. On single integral equations for the transmission problem of acoustics. SIAM J Appl Math 1988;48:307–25.
[17] Kress R. Linear integral equations. New York: Springer; 1989.
[18] Kress R. On the numerical solution of a hypersingular integral equation in scattering theory. J Comput Appl Math 1995;61:345–60.
[19] Leis R. Zur Dirichletschen randwertaufabe des auenraumes der schwingungsgleichung. Math Zeit 1965;90:205–11 English Translation.
[21] Panich IO. On the question of solvability of the exterior boundary value problem for the wave equation and Maxwell's equation. Uspekhi Mat Nauk (Russian Math Surv) 1965;20(1):221–6.
[22] Singh KM, Tanaka M. Analytical evaluation of weakly singular integrals for Helmholtz equation. Trans Jpn Soc Comput Eng Sci 1999;1:161–6.
[23] Song JM, Chew WC. FMM and MLFMA in 3D and fast Illinois solver code. In: Chew WC, Jin JM, Michielssen E, Song JMM, editors. In: Fast and efficient algorithms in computational electromagnetics. Norwood, MA: Artech House; 2001.
[25] Zaman SI. A comprehensive review of boundary integral formulations of acoustic scattering problems. Sci Technol Special Rev 2000:281–310.
[26] Zhang C, JL, Raizen MG, Niu Q. Quantum chaos of bogoliubov waves for a Bose–Einstein condensate in stadium billiards, Phys Rev Lett 2004;93:074101.